Date of publication xxxx 00, 0000, date of current version xxxx 00, 0000.

Digital Object Identifier 10.1109/TQE.2020.DOI

Quantum Feature Refraction: Can Variational Quantum Circuits Enhance Classical Features and Leverage NISQ-Era Noise as Regularization?

CHRISTOPHER W. CLARK, MS[1]

[1]University of Colorado School of Medicine, 13001 E 17th Pl, Aurora, CO 80045, USA (email: christopher.w.clark@cuanschutz.edu)

Corresponding author: Christopher W. Clark (email: christopher.w.clark@cuanschutz.edu).

No financial support to declare

ABSTRACT This work investigates whether variational quantum circuits (VQCs) can effectively improve the separability of features extracted from a convolutional neural network (CNN). We insert a parameterized VQC between a frozen ResNet18 and the classification head, extracting probabilities, full complex amplitudes of the quantum state, and entire density matrices, which are then passed to the multi-layer perceptron classifier. To study the robustness and practical behavior of such hybrid models, we introduce several forms of noisy intermediate-scale quantum (NISQ) noise, including bit-flip, amplitude-damping, and depolarizing channels, directly into the VQC. This enables controlled evaluation of how different noise types affect overall classification performance. We further explore whether quantum noise can function as a form of regularization, analogous to dropout, by preventing overfitting. Experiments are conducted using the MedMNIST dataset, specifically the RetinaMNIST and PneumoniaMNIST subsets, to apply these analyses to real medical data. The results provide empirical insight into the potential of simple VQCs to enrich classical feature extractors and clarify the extent to which NISQ-era noise can be exploited constructively in hybrid quantum–classical learning systems.

INDEX TERMS Deep learning, hybrid quantum–classical models, medical imaging, noisy intermediate-scale quantum devices, variational quantum circuits

I. INTRODUCTION

As advances in quantum hardware bring practical quantum computation closer to reality, research into the advantages and applications of quantum computing has accelerated accordingly [1]. Few-qubit quantum processors are now commercially accessible via the cloud and are capable of running simple quantum algorithms [2]. However, the technical challenges of implementing large-scale, fault-tolerant quantum computers have only been partially overcome; processors on the order of thousands of qubits remain under active development [3]. As a result, current devices are limited to intermediate-scale systems that are highly susceptible to noise [4], [5], commonly referred to as the *Noisy Intermediate-Scale Quantum* (NISQ) era [5].

In this work, we investigate the integration of *Variational Quantum Circuits* (VQCs), parameterized quantum circuits that can be trained using standard machine learning optimization methods [6], into a conventional deep learning pipeline for medical image classification. We use a pretrained, frozen *Convolutional Neural Network* (CNN) encoder [7] to extract classical features, and then either (i) pass those features through a VQC prior to the final classification head or (ii) treat the VQC itself as the final classification layer. Because we simulate the VQC, we can access the full quantum state and extract transformed representations in the form of measurement probabilities, full complex amplitudes, and density matrices. We further inject standard NISQ-era noise channels, including bit-flip, amplitude-damping, and depolarizing noise, into the feature-extraction VQC and into the VQC classifier to study how noise affects generalization and to explore whether quantum noise can act as a regularizer. Experiments are conducted on the RetinaMNIST and PneumoniaMNIST datasets from MedMNIST [8] to evaluate performance on real medical imaging data.

Motivated by prior work on noise as a regularizer in quantum models and on quantum circuits as feature enhancers (found in Section II), we formulate the following hypotheses. First, in a direct comparison, a classical-only model with a large, fully connected head will outperform a VQC-based classifier, due to the substantial difference in the number of trainable parameters. Second, features derived from full complex amplitudes will provide more discriminative information than features based solely on measurement probabilities. Third, models with moderate quantum noise will outperform noiseless models up to a certain noise level, consistent with a regularization effect. Finally, augmenting classical features with VQC-transformed features will improve downstream classification performance compared to using the classical encoder alone.

The primary contributions of this paper are as follows:

1) We integrate VQCs into a deep learning pipeline as feature transformers and as full classifiers, enabling controlled comparisons against classical baselines.
2) We extract and analyze three forms of quantum-derived feature representations: measurement probabilities, full complex amplitudes, and density matrices made possible through simulation.
3) We introduce NISQ-era noise channels (bit-flip, amplitude-damping, and depolarizing) into the VQC and evaluate their effects on classification performance.
4) We assess whether quantum noise can function as a regularizer for hybrid models, analogous to dropout, and identify noise levels that preserve or degrade downstream performance.
5) We conduct experiments on medical imaging benchmarks (RetinaMNIST and PneumoniaMNIST), providing empirical insight into the practical feasibility of hybrid quantum–classical models in real-world classification tasks.

The remainder of this paper is organized as follows: Section II provides a literature review of quantum machine learning more generally, in medicine, specific experiments with VQCs as feature extractors, and noise in quantum circuits. Section III describes the model architectures, datasets, and experimental setup. Section IV presents the results. Section V discusses the results and implications of this work, and Section VI provides next steps and concludes the paper.

II. BACKGROUND AND LITERATURE REVIEW

Though still a nascent field, *Quantum Machine Learning* (QML) is being actively explored for both theoretical and near-term practical applications, including in medicine [9], [10]. Researchers have proposed quantum analogs of machine learning algorithms, spanning both traditional and modern deep learning paradigms. Early efforts focused on adapting non-deep learning models [11]–[13] and have moved to quantum-enhanced deep-learning approaches [14]–[21].

Though all recent innovations, the opportunities QML provides have spurred the exploration and application of these techniques to questions in biology, medicine, and other healthcare settings [22], with several papers providing a summary of the current state of the field [10], [23]–[25].

The addition of a VQC as a feature extractor layer has been explored before for image classification [15], though this was not trainable. However, quantum-classical hybrid models with trainable parameters, as in our setup, have also garnered attention in different contexts [26]

Despite these successes, the ever-present specter of noise in these systems has commanded considerable attention to understand the effects of models trained under realistic conditions [27] and ways to diminish the negative aspects of NISQ-era noise [28]. Unfortunately, "Whether potential advantages of QML can be retained in the presence of noise is largely unaddressed in all studies." [23]. Not all noise is negative, though, as some kinds, such as amplitude damping, can even *improve* quantum reservoir computing models [29] and act as a form of regularization [30].

III. METHODS

A. VARIATIONAL QUANTUM CIRCUITS

VQCs are quantum circuits characterized by trainable parameters and are optimized using classical gradient-based methods [6]. A VQC typically consists of three components: (i) a feature-encoding map that embeds classical data into a quantum state, (ii) layers of trainable single-qubit rotations and entangling operations, and (iii) a measurement stage that extracts classical information for downstream tasks.

B. VQC ARCHITECTURE USED IN THIS WORK

Figure 1 illustrates the two-layer VQC employed in our experiments. Each layer applies parameterized $R_y(\theta)$ rotations to all qubits, followed by a ring of CNOT gates to introduce entanglement. Between layers, we insert configurable quantum noise channels for our regularization experiments.

C. ENCODING

To apply quantum computation to a classical learning task, data must be mapped into a quantum state through an encoding, or *feature map*. In this work, we use *amplitude encoding*, which embeds a d-dimensional real vector $\mathbf{x} \in \mathbb{R}^d$ into the amplitudes of a q-qubit quantum state [6], [31]. The components of $\mathbf{x}$ are normalized and assigned to the computational basis:

$$|\phi(\mathbf{x})\rangle = \sum_{i=0}^{2^q-1} \frac{x_i}{\|\mathbf{x}\|} |i\rangle . \tag{1}$$

In our experiments, the 512-dimensional feature vector extracted from the frozen ResNet18 encoder is embedded into $q = 9$ qubits.

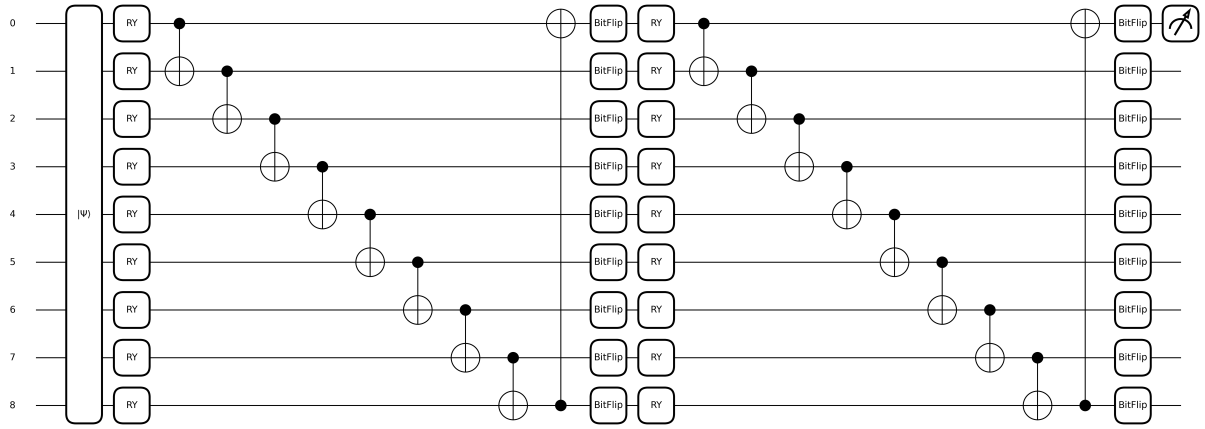

FIGURE 1: VQC architecture consisting of trainable single-qubit rotations, CNOT entangling operations, and optional noise channels between layers.

D. PARAMETERIZED AND ENTANGLING GATES

Trainable single-qubit operations in the VQC are implemented using the $R_y(\theta)$ rotation gate:

$$R_y(\theta) = \begin{bmatrix} \cos\left(\frac{\theta}{2}\right) & -\sin\left(\frac{\theta}{2}\right) \\ \sin\left(\frac{\theta}{2}\right) & \cos\left(\frac{\theta}{2}\right) \end{bmatrix}, \tag{2}$$

where θ is a trainable parameter updated via classical optimization methods.

Entanglement is introduced using the controlled-NOT gate, written in projector form as

$$\text{CNOT} = |0\rangle\langle 0| \otimes I + |1\rangle\langle 1| \otimes X, \tag{3}$$

which applies an X operation to the target qubit when the control qubit is in the $|1\rangle$ state.

The VQC alternates layers of $R_y(\theta)$ rotations and CNOT gates arranged in a ring topology, each qubit entangled with the subsequent and the final entangled with the first.

E. MEASUREMENT

The circuit output is obtained by measuring one or more qubits to produce probabilities $[P(0), P(1)]$ corresponding to the likelihood of observing $|0\rangle$ or $|1\rangle$. These are interpreted as class probabilities, allowing the model to be trained as normally using cross-entropy loss. Formally, the circuit defines a parameterized function:

$$\hat{h}(\mathbf{x}; \boldsymbol{\theta}) = \langle \phi(\mathbf{x}) | U_{\boldsymbol{\theta}}^{\dagger} \hat{O} U_{\boldsymbol{\theta}} | \phi(\mathbf{x}) \rangle,$$

where $U_{\boldsymbol{\theta}}$ is the parameterized unitary (VQC) and $\hat{O}$ the observable being measured [6].

F. NOISY INTERMEDIATE-SCALE QUANTUM NOISE

In the presence of noise, circuit evolution becomes non-unitary and is described using the *operator-sum representation*. A noise channel $\mathcal{E}$ acts on the density matrix $\rho = |\phi(\mathbf{x})\rangle\langle\phi(\mathbf{x})|$ through Kraus operators $\{E_k\}$ [32]:

$$\mathcal{E}(\rho) = \sum_k E_k \rho E_k^{\dagger}.$$

In our model, each variational layer $U_l(\boldsymbol{\theta}_l)$ is followed by a noise channel $\mathcal{E}_l$, producing

$$\rho' = (\mathcal{E}_L \circ U_L) \cdots (\mathcal{E}_1 \circ U_1)(\rho_{\mathbf{x}}),$$

and measurement proceeds as in the noiseless case.

We employ three standard NISQ-era noise channels:

Bit-flip noise

Models classical bit errors with probability p:

$$\mathcal{E}_{\text{bit}}(\rho) = (1-p)\rho + p\, X\rho X.$$

Amplitude damping

Models irreversible relaxation with rate γ. Its Kraus operators are

$$E_0 = \begin{bmatrix} 1 & 0 \\ 0 & \sqrt{1-\gamma} \end{bmatrix}, \quad E_1 = \begin{bmatrix} 0 & \sqrt{\gamma} \\ 0 & 0 \end{bmatrix},$$

and the channel is

$$\mathcal{E}_{\text{amp}}(\rho) = E_0 \rho E_0^{\dagger} + E_1 \rho E_1^{\dagger}.$$

Depolarizing noise

Random Pauli errors applied with equal probability:

$$\mathcal{E}_{\text{depol}}(\rho) = (1-p)\rho + \frac{p}{3}(X\rho X + Y\rho Y + Z\rho Z).$$

G. DATA

Our datasets are RetinaMNIST and PneumoniaMNIST from MedMNIST [8]. Each consist of 28×28 images, with PneumoniaMNIST being grayscale two-class images and RetinaMNIST three-channel, five-class images. As RetinaMNIST does not have many for the final class, class 3 and 4

were combined for a "severe" glaucoma versus class 0, "no glaucoma". PneumoniaMNIST natively has 1,214 images class 0 and 3,494 in class 1, while RetinaMNIST, with class 3 and 4 combined, has 486 images in class 0 and 260 images for class 1. To ensure balanced learning, we undersample all splits (train/validation/test) to the minority class. The training split is further subsampled to a maximum of 1,000 examples. This yields 520 training images for RetinaMNIST (260 per class) and 1,000 for PneumoniaMNIST (500 per class). Validation and test splits use all available balanced samples without further subsampling. All experiments use identical datasets across 10 independent runs with different random seeds.

H. EXPERIMENTS STRUCTURE

Our experiments consist of three pipelines. P1 is a standard ResNet18-based deep learning pipeline with a feature extractor and *Multi-Layer Perceptron* (MLP) classifier. P2 inserts a VQC between the ResNet18 feature extractor and the MLP. The three P2 variants differ in how features are extracted from the VQC output state $|\psi\rangle = \sum_i \alpha_i |i\rangle$. In P2a, we use computational-basis probabilities $p_i = |\alpha_i|^2$, producing a 512-dimensional vector. In P2b, we extract the real and imaginary components $\mathfrak{Re}(\alpha_i)$ and $\mathfrak{Im}(\alpha_i)$, yielding a 1024-dimensional vector. In P2c, we introduce noise, resulting in a mixed state with density matrix ρ, and we vectorize its entries along the diagonal and upper-triangle $\mathfrak{Re}(\rho_{ij}), \mathfrak{Im}(\rho_{ij})$, giving $512 \times 512 = 262{,}144$ features.

Pipeline P3 removes the MLP entirely and treats the VQC as the classifier by measuring qubit q_0 in the computational (Z) basis to obtain the class probabilities $(P(|0\rangle), P(|1\rangle))$.

For P1 and P2, the ResNet18 or VQC feature vector is fed into an MLP that reduces it to 256 features and then outputs two logits for cross-entropy (to keep it similar to how the VQC outputs probabilities). A dropout layer is optionally in the MLP after dimensionality reduction to 256 and ReLU with $p_{\text{dropout}} \in \{0.0, 0.1, 0.2, 0.3, 0.4, 0.5, 0.9\}$ only for the non-VQC pipeline. Noise channels (bit flip, amplitude damping, depolarizing) use $p_{\text{noise}} \in \{0.01, 0.03, 0.05, 0.10, 0.20, 0.30\}$.

Each experiment is run 10 times to capture variance. Training uses default Adam with dual learning rates $\eta_{\text{VQC}} = 0.1$ and $\eta_{\text{MLP}} = 0.001$, batch size 4, 25 epochs, and early stopping after 5 epochs without improvement.

A graphic of the overall structure is found in Fig. 2

IV. RESULTS

We present the following results from baselines to the most important findings of our work. In each figure, we provide the PneumoniaMNIST to the left and RetinaMNIST to the right, except in the case of the noise comparison, in which case PneumoniaMNIST is on top and RetinaMNIST is on bottom. Each graphic, where applicable, shows the p-value from applying Student's t-test to the set of 10 AUCs in each instance.

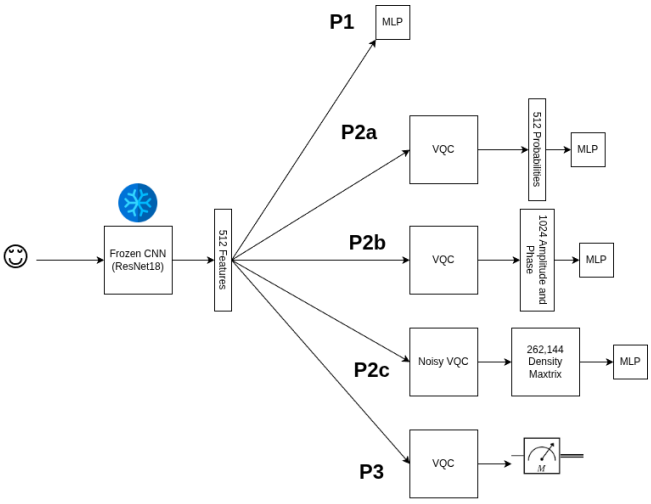

FIGURE 2: Schematic of our three pipelines

A. CLASSICAL VS QUANTUM CLASSIFICATION PERFORMANCE

Figure 3 compares the baseline classical classifier (P1 with dropout $p = 0$) against the quantum classifier (P3 without noise). The classical approach significantly outperforms quantum classification on both datasets ($p < 0.001$). On PneumoniaMNIST, P1 achieves AUC of 0.938 ± 0.005 compared to P3's 0.665 ± 0.071. Similarly, on RetinaMNIST, P1 reaches 0.873 ± 0.006 while P3 achieves 0.782 ± 0.063.

When including optimal regularization (Fig. 4), the performance gap narrows but classical methods maintain their advantage. P1 with optimal dropout continues to outperform P3 with optimal noise on both datasets. This suggests that while noise provides some benefit to quantum classifiers, it is insufficient to close the performance gap with classical baselines.

B. IMPACT OF FULL STATE INFORMATION IN QUANTUM FEATURE REFRACTION

Figure 5 demonstrates a critical finding: quantum features that preserve phase information (P2b with complex amplitudes) significantly outperform those using only probability information (P2a). On PneumoniaMNIST, P2b achieves AUC of 0.919 ± 0.010 compared to P2a's 0.855 ± 0.069 ($p = 0.010$). RetinaMNIST shows a similar pattern with P2b at 0.842 ± 0.028 versus P2a at 0.776 ± 0.079 ($p = 0.023$).

This performance improvement demonstrates that the imaginary components of quantum amplitudes contain discriminative information essential for classification. Discarding phase information by computing only probabilities results in significant information loss.

C. QUANTUM NOISE AS REGULARIZATION

Figures 6 and 7 reveal an unexpected finding: optimal noise levels vary systematically with task difficulty. For the easier task (PneumoniaMNIST with 4,708 training samples), opti-

mal noise is low ($p \approx 0.01$) across all three noise types. The best configuration achieves AUC of 0.942 ± 0.005.

In contrast, the harder task (RetinaMNIST with only 520 training samples) benefits from higher noise levels ($p = 0.03 - 0.1$), reaching AUC of 0.870 ± 0.014. This suggests quantum noise acts as adaptive regularization, with the optimal level scaling inversely with dataset size and task difficulty. Notably, all three noise types achieve similar peak performance when optimally tuned, suggesting the regularization benefit is robust to the specific noise mechanism.

D. QUANTUM-CLASSICAL PERFORMANCE PARITY

Figure 8 presents the main comparison, the best classical model (P1) versus the best quantum-enhanced model (P2d with optimal noise) across all configurations. On PneumoniaMNIST, quantum slightly leads (0.942 ± 0.005 vs 0.938 ± 0.005, $p = 0.059$), while on RetinaMNIST, classical marginally leads (0.873 ± 0.006 vs 0.870 ± 0.014, $p = 0.588$).

Critically, neither difference is statistically significant, though PneumoniaMNIST *does* approach the $p < 0.05$ level. This demonstrates quantum-classical parity. When properly designed, quantum-enhanced models achieve comparable performance to classical baselines but do not provide a clear advantage for these medical imaging tasks.

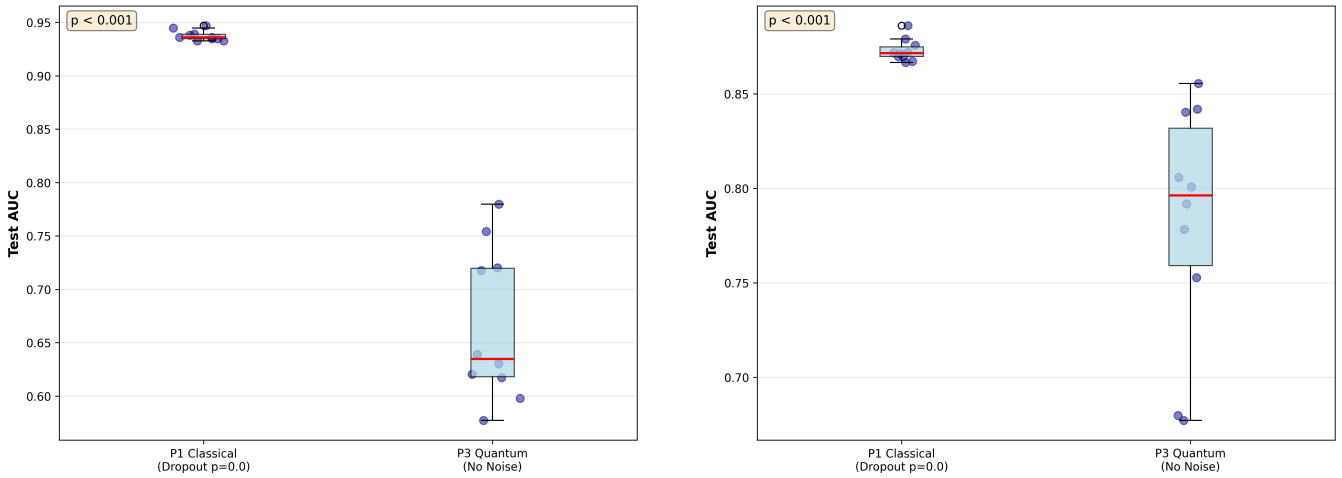

FIGURE 3: Classical (P1, Dropout $p = 0$) vs Quantum Classifier (P3, No Noise). *Left*: PneumoniaMNIST. *Right*: RetinaMNIST. Classical significantly outperforms direct quantum classification ($p < 0.001$).

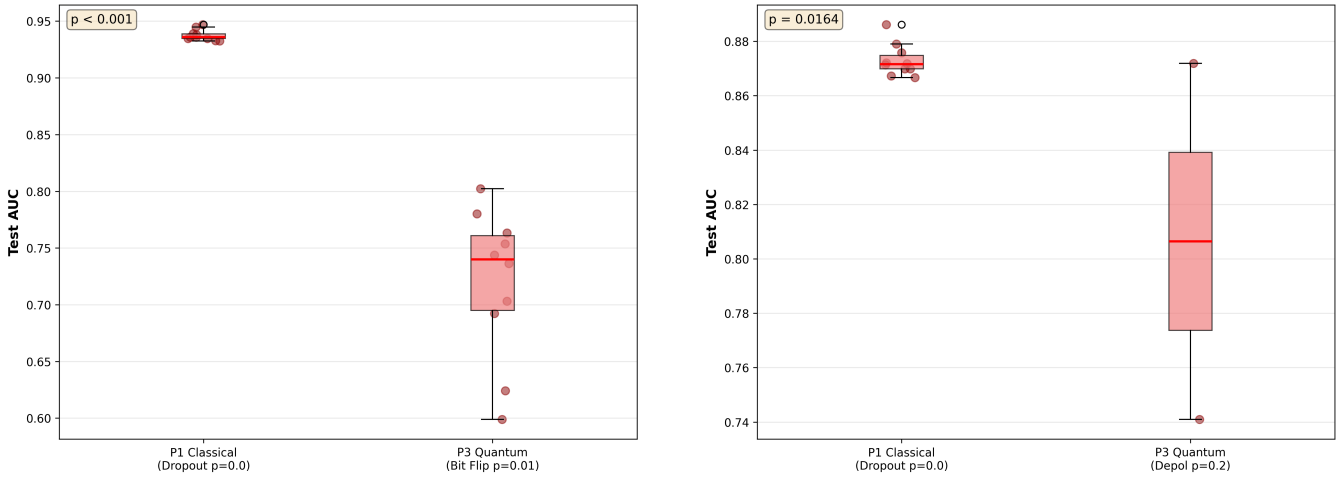

FIGURE 4: Best classical (P1 with optimal dropout) vs best quantum classifier (P3 with optimal noise). *Left*: PneumoniaMNIST. *Right*: RetinaMNIST. Classical maintains advantage even with regularization.

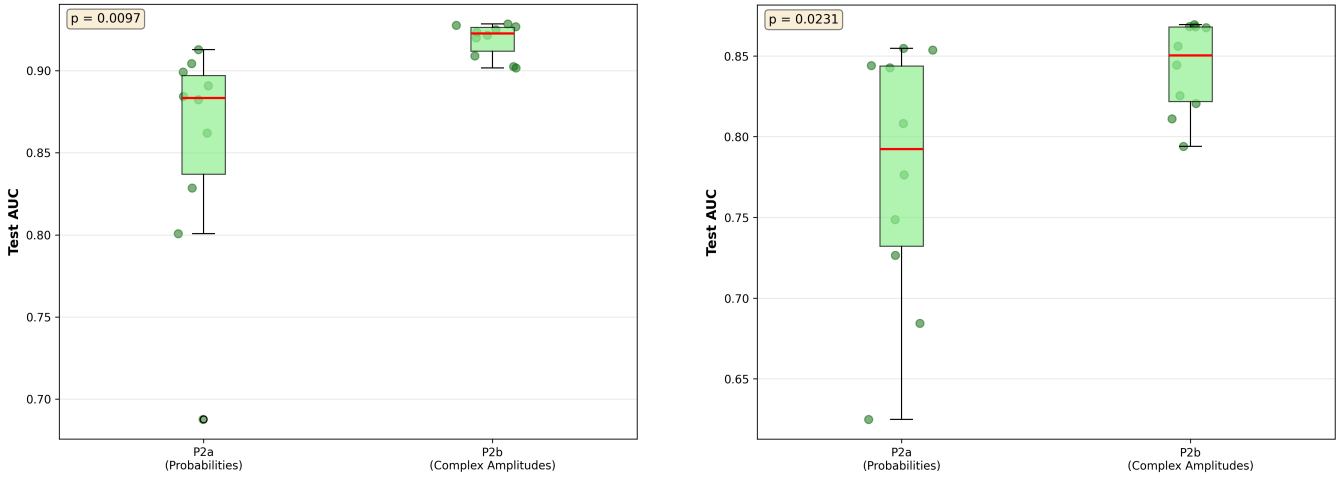

FIGURE 5: Quantum feature extraction methods. *Left*: PneumoniaMNIST. *Right*: RetinaMNIST. P2b (complex amplitudes) significantly outperforms P2a (probabilities only), demonstrating phase information is critical.

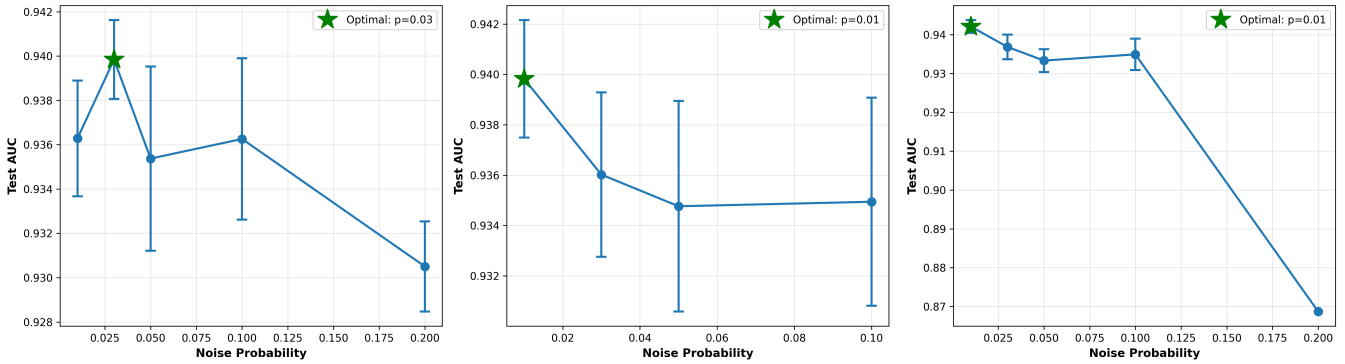

FIGURE 6: Performance across noise types and intensities for PneumoniaMNIST. From left to right, we have amplitude damping, bit flipping, and depolarization. Optimal noise is low ($p \approx 0.01$) for the easier task. All noise types perform similarly at optimal levels.

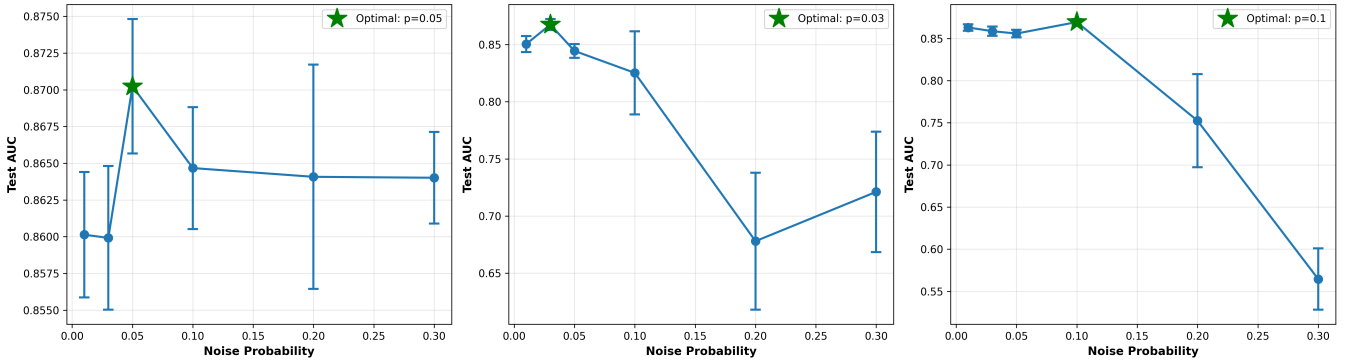

FIGURE 7: Performance across noise types and intensities for RetinaMNIST. From left to right, we have amplitude damping, bit flipping, and depolarization. Optimal noise is higher ($p = 0.03 - 0.1$) for the harder task, suggesting adaptive regularization.

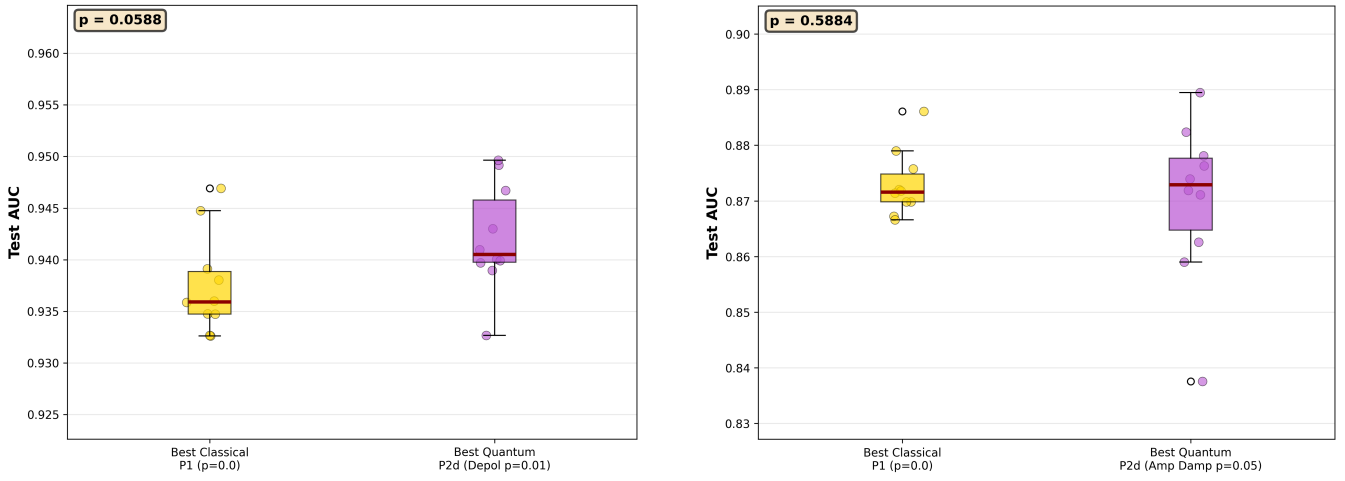

FIGURE 8: Best classical vs best quantum-enhanced model. *Left*: PneumoniaMNIST (0.942 vs 0.938, $p = 0.059$). *Right*: RetinaMNIST (0.873 vs 0.870, $p = 0.588$).

V. DISCUSSION

In a direct head-to-head comparison between a classical and VQC classifier, Section IV-A, particularly Fig. 3, demonstrate a clear advantage of the classical classifier. However, we note that this *could* be explained by the parameter counts, as the VQC has only 20 parameters to the MLP's 131,585, arguing that parameter count is still a main driver for performance.

Focusing on the viability of using a VQC to enhance previously extracted features in a noiseless environment, Section IV-B demonstrates a predictable performance increase when we provide the entire set of complex amplitudes. This improves performance and variance, as in both datasets the 10 runs for the models provided the complex amplitudes are far tighter than the probability-only models (though additional statistical testing, such as Levene's test for equality of variances [33], would be needed to confirm this). Though the performance increases due to the additional phase information provided by the complex parts of the coefficients are not such a surprise, the reduction in variance deserves additional exploration.

From Section IV-C, we see quantum noise acts as adaptive regularization when passing the entire density matrix to the MLP classification head, with the optimal level scaling inversely with dataset size and task difficulty. Notably, all three noise types achieve similar peak performance when optimally tuned, suggesting the regularization benefit is robust to the specific noise mechanism, though as noise increases, particularly depolarization, performance begins to suffer. However, we note that this is not enough to overcome, by itself, the advantages of the classical, parameter-rich pipeline when pitted against the simpler, noisy VQC classifier, as seen in Fig. 4.

As the most important test, whether a VQC-enhanced pipeline can achieve or surpass a classical one, Section IV-D demonstrates that the best-performing VQC-enhanced pipeline, one in which the noisy VQC acts not as a classifier but as a feature extractor passing the entire density matrix to the MLP, we find that this VQC-enhanced pipeline exceeds on average the classical pipeline. However, we caution two points, that the p-value does not reach the 0.05 level (though it approaches this in the PneumoniaMNIST case), and as the MLP is now receiving a very large set of features from the full density matrix, the number of parameters in the MLP classifier has similarly increased. Previously, in the comparison between the baseline classical classifier and the VQC classifier, we mentioned this parameter difference as a confounding factor, and we must again highlight this, but in the opposite direction, with the VQC-enhanced pipeline now having far more parameters overall. Additional experiments are needed to determine if this performance can be attributed to the VQC or merely that we now have far more parameters with which to analyze the incoming features.

VI. CONCLUSION, LIMITATIONS, AND NEXT STEPS

From these results, we are ready to answer our hypotheses and determine the next steps. Section IV-A provides statistically significant evidence for our first hypothesis, that a classical classier outperforms a VQC classifier on pre-extracted features. Sections IV-B, and IV-C answer our second hypothesis, that more information from the VQC, either complex amplitudes in the case of the no-noise models or full density matrices from the noisy VQC feature enhancers, results in better performance when given to an MLP classifier. Our third hypothesis, that noise acts as a regularizer (up to a point) is supported by Section IV-C and Fig. 4 for both the VQC as a feature enhancer or classifier, though more direct statistical comparisons between different permutations of these noisy models would provide more evidence for this claim. Finally, Section IV-D argues for our final hypothesis, that VQC-transformed features will result in better classification, though we caution that the confounding factor of large parameter differences needs to be addressed and care needs to be taken to achieve an acceptable level of statistical significance in both datasets.

Further analyses are needed to clarify remaining questions, such as how these various permutations of noise, features, and classification affect model stability, as graphical evidence suggests this, but statistical testing is needed. The role that parameter count plays also needs to be understood, especially for hypotheses one and four. Additionally, claims about the optimal level of noise scaling with task difficulty are supported by this work, but more datasets could strengthen this argument. Finally, and most importantly, our results indicate that VQCs do generate linearly separable quantum representations, but because only a tiny fraction of this information is accessible through physical measurement of the first qubit, practical VQC classifiers cannot exploit the internal structure visible to the MLP in simulation using this method. This gap between available and extractable information suggests that measurement, not expressivity, may be the dominant performance bottleneck in current NISQ-era quantum models and additional research is needed to learn how to properly extract and use the representations generated by a real VQC.

REFERENCES

[1] T. D. Ladd, F. Jelezko, R. Laflamme, Y. Nakamura, C. Monroe, and J. L. O'Brien, "Quantum computers," nature, vol. 464, no. 7285, pp. 45–53, 2010.
[2] C. Vu, "Ibm makes quantum computing available on ibm cloud to accelerate innovation," IBM News Room, vol. 84, 2016.
[3] IBM, "Ibm quantum technology overview and roadmap," https://www.ibm.com/quantum/technology, 2025, accessed: 2025-05-28.
[4] E. National Academies of Sciences, Medicine et al., Quantum computing: progress and prospects, 2018.
[5] J. Preskill, "Quantum Computing in the NISQ era and beyond," Quantum, vol. 2, p. 79, Aug. 2018. [Online]. Available: https://doi.org/10.22331/q-2018-08-06-79
[6] M. Benedetti, E. Lloyd, S. Sack, and M. Fiorentini, "Parameterized quantum circuits as machine learning models," Quantum science and technology, vol. 4, no. 4, p. 043001, 2019.
[7] Y. LeCun, Y. Bengio, and G. Hinton, "Deep learning," nature, vol. 521, no. 7553, pp. 436–444, 2015.

[8] J. Yang, R. Shi, D. Wei, Z. Liu, L. Zhao, B. Ke, H. Pfister, and B. Ni, "Medmnist v2: A large-scale lightweight benchmark for 2d and 3d biomedical image classification," Scientific Data, vol. 10, no. 1, p. 41, 2023.

[9] M. Klusch, J. Lässig, D. Müssig, A. Macaluso, and F. K. Wilhelm, "Quantum artificial intelligence: A brief survey," KI-Künstliche Intelligenz, pp. 1–20, 2024.

[10] S. Chakraborty, "A study on quantum neural networks in healthcare 5.0," arXiv preprint arXiv:2412.06818, 2024.

[11] P. Rebentrost, M. Mohseni, and S. Lloyd, "Quantum support vector machine for big data classification," Physical review letters, vol. 113, no. 13, p. 130503, 2014.

[12] I. Kerenidis, J. Landman, A. Luongo, and A. Prakash, "q-means: A quantum algorithm for unsupervised machine learning," Advances in neural information processing systems, vol. 32, 2019.

[13] S. Lloyd, M. Mohseni, and P. Rebentrost, "Quantum principal component analysis," Nature physics, vol. 10, no. 9, pp. 631–633, 2014.

[14] I. Cong, S. Choi, and M. D. Lukin, "Quantum convolutional neural networks," Nature Physics, vol. 15, no. 12, pp. 1273–1278, 2019.

[15] M. Henderson, S. Shakya, S. Pradhan, and T. Cook, "Quanvolutional neural networks: powering image recognition with quantum circuits," Quantum Machine Intelligence, vol. 2, no. 1, p. 2, 2020.

[16] E. A. Cherrat, I. Kerenidis, N. Mathur, J. Landman, M. Strahm, and Y. Y. Li, "Quantum vision transformers," arXiv preprint arXiv:2209.08167, 2022.

[17] R. Guarasci, G. De Pietro, and M. Esposito, "Quantum natural language processing: Challenges and opportunities," Applied sciences, vol. 12, no. 11, p. 5651, 2022.

[18] N. Meyer, C. Ufrecht, M. Periyasamy, D. D. Scherer, A. Plinge, and C. Mutschler, "A survey on quantum reinforcement learning," arXiv preprint arXiv:2211.03464, 2022.

[19] H.-L. Huang, Y. Du, M. Gong, Y. Zhao, Y. Wu, C. Wang, S. Li, F. Liang, J. Lin, Y. Xu et al., "Experimental quantum generative adversarial networks for image generation," Physical Review Applied, vol. 16, no. 2, p. 024051, 2021.

[20] S. Y. Chang, S. Thanasilp, B. L. Saux, S. Vallecorsa, and M. Grossi, "Latent style-based quantum gan for high-quality image generation," arXiv preprint arXiv:2406.02668, 2024.

[21] J. Romero, J. P. Olson, and A. Aspuru-Guzik, "Quantum autoencoders for efficient compression of quantum data," Quantum Science and Technology, vol. 2, no. 4, p. 045001, 2017.

[22] F. F. Flöther, "The state of quantum computing applications in health and medicine," Research Directions: Quantum Technologies, vol. 1, p. e10, 2023.

[23] R. S. Gupta, C. E. Wood, T. Engstrom, J. D. Pole, and S. Shrapnel, "A systematic review of quantum machine learning for digital health," npj Digital Medicine, vol. 8, no. 1, p. 237, 2025.

[24] U. Ullah and B. Garcia-Zapirain, "Quantum machine learning revolution in healthcare: a systematic review of emerging perspectives and applications," IEEE Access, vol. 12, pp. 11 423–11 450, 2024.

[25] A. Marengo and V. Santamato, "Quantum algorithms and complexity in healthcare applications: a systematic review with machine learning-optimized analysis," Frontiers in Computer Science, vol. 7, p. 1584114, 2025.

[26] H. Aslam and F. Holweck, "A hybrid variational quantum circuit approach for stabilizer states classifiers," arXiv preprint arXiv:2511.09430, 2025.

[27] T. Ahmed, M. Kashif, A. Marchisio, and M. Shafique, "Quantum neural networks: A comparative analysis and noise robustness evaluation," arXiv preprint arXiv:2501.14412, 2025.

[28] M. U. Khan, M. A. Kamran, W. R. Khan, M. M. Ibrahim, M. U. Ali, and S. W. Lee, "Error mitigation in the nisq era: Applying measurement error mitigation techniques to enhance quantum circuit performance," Mathematics, vol. 12, no. 14, p. 2235, 2024.

[29] L. Domingo, G. Carlo, and F. Borondo, "Taking advantage of noise in quantum reservoir computing," Scientific Reports, vol. 13, no. 1, p. 8790, 2023.

[30] W. Somogyi, E. Pankovets, V. Kuzmin, and A. Melnikov, "Method for noise-induced regularization in quantum neural networks," arXiv preprint arXiv:2410.19921, 2024.

[31] S. Sim, P. D. Johnson, and A. Aspuru-Guzik, "Expressibility and entangling capability of parameterized quantum circuits for hybrid quantum-classical algorithms," Advanced Quantum Technologies, vol. 2, no. 12, p. 1900070, 2019.

[32] K. Kraus, A. Böhm, J. D. Dollard, and W. Wootters, States, Effects, and Operations Fundamental Notions of Quantum Theory: Lectures in Mathematical Physics at the University of Texas at Austin. Springer, 1983.

[33] M. B. Brown and A. B. Forsythe, "Robust tests for the equality of variances," Journal of the American statistical association, vol. 69, no. 346, pp. 364–367, 1974.